insulating state will probably be settled by calculations of lattice dynamical energies. □

Received 10 February; accepted 12 May 1999.

1. Kresse, G. & Hafner, J. *Ab initio* molecular dynamics for liquid metals. *Phys. Rev. B* **47,** RC558–RC561 (1993).
2. Kresse, G. & Furthmüller, J. Efficient iterative schemes for *ab initio* total-energy calculations using a plane-wave basis set. *Phys. Rev. B* **54,** 11169–11186 (1996).
3. Hohenberg, P. & Kohn, W. Inhomogeneous electron gas. *Phys. Rev.* **136,** B864–B871 (1964).
4. Kohn, W. & Sham, L. J. Self-consistent equations including exchange and correlation effects. *Phys. Rev.* **140,** A1133–A1138 (1965).
5. Blöchl, P. E. Projector augmented-wave method. *Phys. Rev. B* **50,** 17953–17979 (1994).
6. Boettger, J. C. & Trickey, S. B. Equation of state and properties of lithium. *Phys. Rev. B* **32,** 3391–3398 (1985).
7. Perdew, J. P. *et al.* Atoms, molecules, solids, and surfaces: applications of the generalized gradient approximation for exchange and correlation. *Phys. Rev. B* **46,** 6671–6687 (1992).
8. Jaffe, J. E. *et al.* Gaussian-basis LDA and GGA calculations for alkali-metal equations of state. *Phys. Rev. B* **57,** 11834–11837 (1998).
9. Overhauser, A. W. Crystal structure of lithium at 4.2 K. *Phys. Rev. Lett.* **53,** 64–65 (1984).
10. Liu, A. Y. & Cohen, M. L. Electron-phonon coupling in bcc and 9R lithium. *Phys. Rev. B* **44,** 9678–9684 (1991).
11. Needs, R J., Martin, R. M. & Nielsen, O. H. Total-energy calculations of the structural properties of the group-V element arsenic. *Phys. Rev. B* **33,** 3778–3784 (1986).
12. Johnson, K. A. & Ashcroft, N. W. *Nature* (submitted).
13. Straus, D. M. & Ashcroft, N. W. Self-consistent structure of metallic hydrogen. *Phys. Rev. Lett.* **38,** 415–418 (1977).
14. Natoli, V., Martin, R. M. & Ceperly, D. Crystal structure of molecular hydrogen at high pressure. *Phys. Rev. Lett.* **74,** 1601–1604 (1984).
15. Overhauser, A. W. Exchange and correlation instabilities of simple metals. *Phys. Rev.* **167,** 691-698 (1968).
16. Richardson, C. F. & Ashcroft, N. W. High-temperature superconductivity in metallic hydrogen: electron-electron enhancements. *Phys. Rev. Lett.* **78,** 118–121 (1997).
17. Siringo, F., Pucci, R. & Angilella, G. G. N. Are the light alkali metals still metals under high pressure? *High Pressure Res.* **15,** 255–262 (1997).
18. Moulopoulos, K. & Ashcroft, N. W. Scaling relations for two-component charged systems: Application to metallic hydrogen. *Phys. Rev. B* **41,** 6500–6519 (1990).
19. Moulopoulos, K. & Ashcroft, N. W. Generalized Coulomb pairing in the condensed state. *Phys. Rev. Lett.* **66,** 2915–2918 (1991).
20. Moulopoulos, K. & Ashcroft, N. W. Coulomb interactions and generalized pairing in condensed matter. *Phys. Rev. B* (in the press).
21. Vanderbilt, D. Soft self-consistent pseudopotentials in a generalized eigenvalue formalism. *Phys. Rev. B* **41,** 7892–7895 (1990).
22. Kresse, G. & Hafner, J. Norm-conserving and ultrasoft pseudopotentials for first-row and transition elements. *J. Phys. Condens. Matter* **6,** 8245–8257 (1994).
23. Lin, T. H. & Dunn, K. J. High-pressure and low-temperature study of electrical resistance of lithium. *Phys. Rev. B* **33,** 807–811 (1986).
24. Cracknell, A. P. *Landolt-Börnstein: Numerical Data and Functional Relationships in Science and Technology* (eds Hellwege, K.-H. & Olsen, J. L.) Group III, Vol. 13c, 451–462 (Springer, Berlin, 1984).
25. Sherrington, D. & Kohn, W. Frequency-dependent dielectric function of a zero-gap semiconductor. *Phys. Rev. Lett.* **21,** 153–156 (1968).
26. Zittel, W. G. *et al.* Band-reordering effects in the ultra-high-pressure equation of state of lithium. *J. Phys. F* **15,** L247–L251 (1985).
27. Boettger, J. C. & Albers, R. C. Structural phase stability in lithium to ultrahigh pressures. *Phys. Rev. B* **39,** 3010–3014 (1989).
28. Cohen, M. H. Optical constants, heat capacity, and the Fermi surface. *Phil. Mag.* **3,** 762–775 (1958).

Acknowledgements. We thank K. A. Johnson and M. P. Teter for discussions, and we thank G. Kresse, J. Furthmüller and J. Hafner for providing the VASP software. This work was supported by the NSF.

Correspondence and requests for materials should be addressed to N.W.A. (e-mail: nwa@ccmr.cornell.edu).

Observation of shell structure in sodium nanowires

A. I. Yanson*, I. K. Yanson*† & J. M. van Ruitenbeek*

* *Kamerlingh Onnes Laboratorium, Universiteit Leiden, PO Box 9504, NL-2300 RA Leiden, The Netherlands*

† *B. Verkin Institute for Low Temperature Physics and Engineering, National Academy of Sciences, 310164, Kharkiv, Ukraine*

The quantum states of a system of particles in a finite spatial domain in general consist of a set of discrete energy eigenvalues; these are usually grouped into bunches of degenerate or close-lying levels[1], called shells. In fermionic systems, this gives rise to a local minimum in the total energy when all the states of a given shell are occupied. In particular, the closed-shell electronic configuration of the noble gases produces their exceptional stability. Shell effects have previously been observed for protons and neutrons in nuclei, and for clusters of metal atoms[2–4]. Here we report the observation of shell effects in an open system—a sodium metal nanowire connecting two bulk sodium metal electrodes, which are progressively pulled apart. We measure oscillations in the statistical distribution of conductance values, for contact cross-sections containing up to a hundred atoms or more. The period follows the law expected from shell-closure effects, similar to the abundance peaks at 'magic' numbers of atoms in metal clusters[3,4].

Metallic constrictions, in the form of nanowires connecting two bulk metal electrodes, have been studied down to sizes of a single atom in cross-section by means of scanning tunnelling microscopy (STM) and mechanically controllable break-junctions (MCB)[5,6]. By indenting one electrode into another and then separating them, a stepwise decrease in electrical conductance is observed, down to the breakpoint when arriving at the last atom. Each scan of the dependence of conductance G on the elongation d is individual in detail, as the atomic configuration of each contact may be widely different. However, statistically, many scans together produce a histogram of the probability for observing a given conductance value, which is quite reproducible for a given metal and for fixed experimental parameters.

A simple description of the electronic properties of metallic nanowires is expected to work best for monovalent free-electron-like metals. The alkali metals are most suitable, as the bulk electronic states are very well described by free particles in an isotropic homogeneous positive background. In a previous experiment on sodium point contacts[7] a histogram was obtained, which showed pronounced peaks near 1, 3, 5 and 6 times the quantum unit of conductance, $G_0 = 2e^2/h$ (where e is the charge on an electron and h is Planck's constant). This is exactly the series of quantum numbers expected for the conductance through an ideal cylindrical conductor. We have now extended these experiments to higher temperatures and a much wider range of conductance values.

The MCB technique[6] was adapted for the study of nanowires of the highly reactive alkali metals following ref. 7 (see Fig. 1). Scans were taken continuously by ramping the displacement d of the

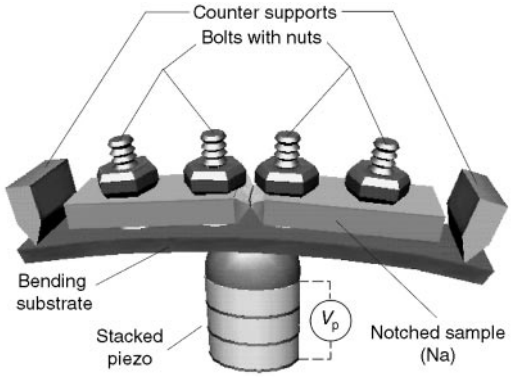

Figure 1 Schematic view of the MCB technique for alkali metals[7]. While immersed in paraffin oil, the sample is pressed onto four 1-mm-diameter brass bolts, which are glued onto the isolated substrate. Current and voltage leads are fixed with nuts onto the bolts. A notch is cut into the sample at the centre. This assembly is mounted inside a vacuum can, which is immersed in liquid helium. By bending the substrate at 4.2 K in vacuum, the sample is broken at the notch. Two fresh surfaces are exposed, and their distance is adjusted by changing the force on the substrate, employing a piezo element for fine control. The temperature of the sample is controlled by a heater and thermometer, which are fixed at the bottom of the substrate. The cryo-pumping action of the low-temperature environment ensures that the surfaces are not polluted by adsorbates. The purity of the sodium metal was at least 99.9%. The conductance was recorded using a standard d.c. voltage bias four-terminal technique, measuring the current with 16-bit resolution. The drift and calibration of the current-to-voltage converter was verified against standard resistors corresponding to 1, 10 and 100 G_0, leading to an overall accuracy in the conductance better than 1% for $G > 10\,G_0$.

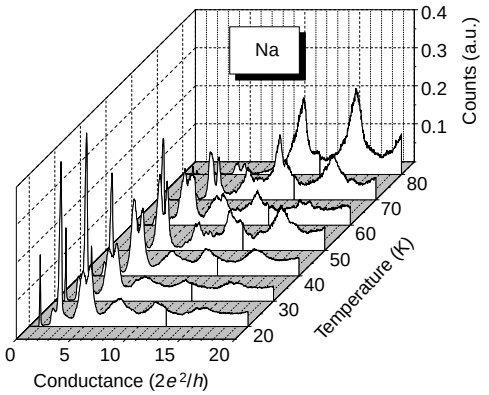

Figure 2 Temperature evolution of sodium histograms in the range from 0 to 20 G_0. The voltage bias was 10 mV and each histogram is constructed from 1,000–2,000 individual scans. The amplitude has been normalized by the total area under each histogram (a.u., arbitrary units).

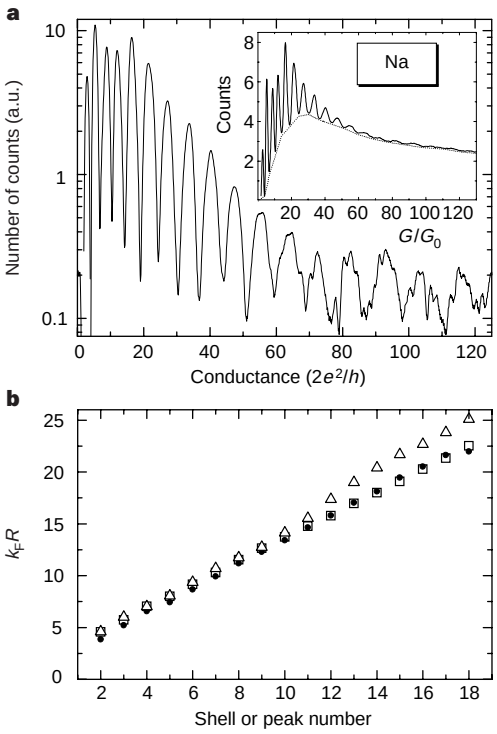

Figure 3 Conductance histograms for sodium, showing evidence for shell structure. **a**, Histogram of the number of times each conductance is observed versus the conductance in units of $G_0 = 2e^2/h$. These data are for sodium at $T = 80$ K and bias voltage $V = 100$ mV, constructed from over 10,000 individual scans. Inset, the raw data and the smooth background (dotted curve); the background is subtracted to give the curve in the main graph. The logarithmic scale for the ordinate axis helps to display the smaller-amplitude features at high conductance values. **b**, Radius of the nanowire at the positions of the maxima in **a** versus peak numbers (open squares), where R is given in units k_F^{-1}. The radii at the peak positions are compared with the radii corresponding to the magic numbers for sodium metal clusters (filled circles)[11] and with those expected from a semi-classical description for the fluctuations in the free energy for the nanowire (open triangles)[18,19].

electrodes with respect to each other, using the piezo-electric driver. Each individual curve of conductance versus displacement, $G(d)$, was recorded in ~0.1 seconds from the highest conductance into the tunnelling regime. Histograms of conductance values were accumulated automatically involving 10^3–10^5 individual scans, and for a number of sample temperatures between 4.2 K and 100 K. Reproducibility and reversibility were verified by periodically returning to the same measuring conditions. Here we present results for sodium, but similar results were obtained for lithium and potassium.

Figure 2 shows the temperature dependence of the histograms for sodium in the range from 0 to 20 G_0. In order to compare different graphs, the amplitude has been normalized by the area under each graph. The histograms at low temperatures and low conductances are similar to those given in ref. 7. We clearly recognize the familiar sharp peaks below 6 G_0, while at higher conductances a number of rather wide maxima are found. With increasing temperature we observe a gradual decrease in amplitude of the lower-conductance peaks, while the high-conductance peaks dramatically sharpen and increase in amplitude.

Our central results are shown in Fig. 3. The histogram for sodium at temperature $T = 80$ K up to $G/G_0 = 120$ is shown in Fig. 3a inset. The smooth background shown by the dotted curve was subtracted, in order to present only the oscillating part; the latter is plotted on a semi-logarithmic scale in the main panel of Fig. 3a. Up to 17 oscillations are observed, at positions which are reproduced well for ~10 different samples. The influence of the procedure of background subtraction on the peak positions is much smaller than the width of the peaks.

The radius, R, of the narrowest cross-section of the nanowire can be obtained from the semi-classical expression for a ballistic wire[8]

$$G/G_0 \approx \left(\frac{k_F R}{2}\right)^2 \left(1 - \frac{2}{k_F R}\right) \quad (1)$$

where k_F is the Fermi wavevector. Using this expression, we calculate the radius of the nanowire at the peak positions (in units of k_F^{-1}); the results are shown in Fig. 3b (open squares) for consecutively numbered peak index i. Thus we observe that the peak positions are periodic as a function of the radius of the wire. This periodicity suggests a comparison of our experimental results with the magic numbers observed for sodium clusters. In the cluster experiments, a remarkable structure was observed in the distribution of cluster sizes produced in a supersonic expansion of sodium metal vapour[3,9–13]. In the spectrum of abundance versus the number of atoms, N, in the cluster, distinct maxima are observed for $N = 2, 8, 20, 40, 58, 92, \ldots$. These 'magic numbers' correspond to clusters having a number of valence electrons (equal to the number of atoms) which just complete a shell, where the wavefunctions are considered as freely propagating waves inside a spherical potential well. The magic numbers are periodically distributed as a function of the radius of the clusters, where the radius is obtained from the number of atoms, N, in the cluster using[3,4] $k_F R = 1.92N^{1/3}$. In Fig. 3b we compare the radii for the cluster magic numbers (filled circles) with the radii corresponding to the peaks in the conductance histogram (open squares). We establish a direct correspondence between preferential values for the conductance in histograms for sodium nanowires, and the cluster magic numbers.

The linear relation between the radii at cluster magic numbers and the shell number arises owing to fluctuations in the density of states as a function of $k_F R$, which in turn give rise to fluctuations in the free energy of the system, $\Omega(R)$. The periods of oscillation can be expressed in terms of semiclassical closed orbits inscribed inside the boundaries of the system[1,4], where the path length L should be an integer multiple of the Fermi wavelength $\lambda_F = 2\pi/k_F$. Fluctuations in the density of states for a free electron nanowire and their influence on the free energy has been recently considered in a number of theoretical papers[14–19]. Using the semiclassical expansion of the free energy for a cylindrical wire[18,19] including only the three lowest-order terms, we calculated the positions of the energy minima, which are plotted as a function of shell number in Fig. 3b (open triangles). The agreement with the experimental points is fairly good, and may be improved taking into account a more realistic shape of the potential well and higher-order contributions.

Our interpretation uses the approximately linear semiclassical relation $G(R)$ between conductance and wire cross-section, equation (1). Corrections may arise from two mechanisms. First, back scattering on defects (or phonons) may shift the peak positions. The fact that strong scattering would tend to smear the peak structure, and the close agreement between the experimental and theoretical periodicity both suggest that this shift is small. Second, the mechanism of level-bunching leading to fluctuations in $\Omega(R)$ should also give rise to fluctuation corrections to $G(R)$, which by itself would lead to peaks in the histograms even for a perfectly smooth distribution of wire diameters. Peaks due to this mechanism would be found at those points where the increase of the conductance with wire diameter is slow, and indeed we believe the peaks at low conductance (near 1, 3 and 6 G_0) are due to this mechanism. However, we argue that the main structure in Fig. 3 is due to the shell structure in $\Omega(R)$.

The main argument in favour of this interpretation comes from the temperature dependence shown in Fig. 2. As in the cluster experiments[11], the electronic shell structure becomes observable at higher temperatures, where the increased mobility of the atoms allows the system to explore a wider range of neighbouring atomic configurations in order to find the local energy minima. At low temperatures, the nanowires are frozen into the shape which evolves from mechanical deformations in the breaking and indenting processes. The decrease in amplitude of the sharp quantization peaks at low conductance can probably be explained by thermally induced breaking of the contact when it consists of only a few atoms. If the fluctuations in $G(R)$ were solely responsible for the observed peak structure, it could be argued that the higher temperature would favour formation of a smoother and longer wire, leading to less backscattering of electrons and less tunnelling corrections, respectively. Backscattering is responsible for the shift to lower values of the conductance peaks near 1, 3, 5 and 6 G_0 (ref. 20), and we find that the position of these peaks does not change with temperature. An indication of the length of the wire may be obtained from the global variation of the conductance with elongation[21], and the time evolution of conductance for fixed elongation[22]. In our experiment, both variations show that the effective wire length decreases for increasing temperature. With these arguments, an interpretation of the temperature dependence of Fig. 2 in terms of $G(R)$ fluctuations alone is ruled out.

The correspondence between the shell structure in clusters and in nanowires can be explained by comparing the energy levels for a three-dimensional spherical potential well and a two-dimensional cylindrical geometry. The levels are obtained from the zeros of the spherical and ordinary Bessel functions, respectively. Apart from a small constant shift, the distribution of levels for the two systems has a very similar structure, with gaps and bunches of levels occurring at the same positions. This explains the striking similarity of the magic radii for the clusters and nanowires observed in Fig. 3b. □

Received 15 January; accepted 29 April 1999.

1. Balian, R. & Bloch, C. Distribution of eigenfrequencies for the wave equation in a finite domain: III. Eigenfrequency density oscillations. *Ann. Phys. (NY)* **69,** 76–160 (1972).
2. Bohr, Å & Mottelson, B. R. *Nuclear Structure* Vol. II (Benjamin, Reading, Massachusetts, 1975).
3. de Heer, W. A. The physics of simple metal clusters: experimental aspects and simple models. *Rev. Mod. Phys.* **65,** 611–676 (1993).
4. Brack, M. The physics of simple metal clusters: self-consistent jellium model and semi-classical approaches. *Rev. Mod. Phys.* **65,** 677–732 (1993).
5. Agraït, N., Rodrigo, J. G. & Vieira, S. Conductance steps and quantization in atomic-size contacts. *Phys. Rev. B* **47,** 12345–12348 (1993).
6. Muller, C. J., van Ruitenbeek, J. M. & de Jongh, L. J. Experimental observation of the transition from weak link to tunnel junction. *Physica C* **191,** 485–504 (1992).
7. Krans, J. M. *et al.* The signature of conductance quantization in metallic point contacts. *Nature* **375,** 767–769 (1995).
8. Torres, J. A., Pascual, J. I. & Sáenz, J. J. Theory of conduction through narrow constrictions in a three-dimensional electron gas. *Phys. Rev. B* **49,** 16581–16584 (1994).
9. Knight, W. D. *et al.* Electronic shell structure and abundances of sodium clusters. *Phys. Rev. Lett.* **52,** 2141–2143 (1984).
10. Martin, T. P. *et al.* Observation of electronic shells and shells of atoms in large Na clusters. *Chem. Phys. Lett.* **172,** 209–213 (1990).
11. Martin, T. P. *et al.* Electronic shell structure of laser-warmed Na clusters. *Chem. Phys. Lett.* **186,** 53–57 (1991).
12. Bjørnholm, S. *et al.* Mean-field quantization of several hundred electrons in sodium metal clusters. *Phys. Rev. Lett.* **65,** 1627–1630 (1990).
13. Pedersen, J. *et al.* Observation of quantum supershells in clusters of sodium atoms. *Nature* **353,** 733–735 (1991).
14. Stafford, C. A., Baeriswyl, D. & Bürki, J. Jellium model of metallic nanocohesion. *Phys. Rev. Lett.* **79,** 2863–2866 (1997).
15. Kassubek, F., Stafford, C. A. & Grabert, H. Force, charge, and conductance of an ideal metallic nanowire. *Phys. Rev. B* **59,** 7560–7574 (1999).
16. van Ruitenbeek, J. M., Devoret, M. H., Esteve, D. & Urbina, C. Conductance quantization in metals: The influence of subband formation on the relative stability of specific contact diameters. *Phys. Rev. B* **56,** 12566–12572 (1997).
17. Yannouleas, C. & Landman, U. On mesoscopic forces and quantized conductance in model metallic nanowires. *J. Phys. Chem. B* **101,** 5780–5783 (1997).
18. Yannouleas, C., Bogachek, E. N. & Landman, U. Energetics, forces, and quantized conductance in jellium-modeled metallic nanowires. *Phys. Rev. B* **57,** 4872–4882 (1998).
19. Höppler, C. & Zwerger, W. Quantum fluctuations in the cohesive force of metallic nanowires. *Phys. Rev. B* **59,** R7849–R7851 (1999).
20. Ludoph, B. *et al.* Evidence for saturation of channel transmission from conductance fluctuations in atomic-size point contacts. *Phys. Rev. Lett.* **82,** 1530–1533 (1999).
21. Untiedt, C. *et al.* Fabrication and characterization of metallic nanowires. *Phys. Rev. B* **56,** 2154–2160 (1997).
22. Gai, Z. *et al.* Spontaneous breaking of nanowires between a STM tip and the Pb(110) surface. *Phys. Rev. B* **58,** 2185–2190 (1998).

Acknowledgements. We thank L. J. de Jongh for his continuous support.

Correspondence and requests for materials should be addressed to J.M.v.R. (e-mail: Ruitenbe@Phys.LeidenUniv.nl).

Chain conformation in ultrathin polymer films

Ronald L. Jones*, Sanat K. Kumar*, Derek L. Ho†, Robert M. Briber† & Thomas P. Russell‡

** Department of Materials Science and Engineering, Pennsylvania State University, University Park, Pennsylvania 16803, USA*
† Department of Materials and Nuclear Engineering, University of Maryland, College Park, Maryland 20740, USA
‡ Polymer Science and Engineering Department, University of Massachusetts, Amherst, Massachusetts 01003, USA

Polymer thin films are used in a variety of technological applications—for example, as paints, lubricants and adhesives. Theories that predict the properties of molten polymers in confined geometries (as in a thin film) generally start from the premise that the chains maintain their unperturbed gaussian conformation in the direction parallel to the surface[1–5]. This assumption has been questioned, however, by recent experiments[6–8]. Here we use small-angle neutron scattering to characterize the chain structure and conformation in ultrathin (less than 100 nm) polymer films. The conformation can be deduced directly from the scattering from mixtures of protonated and perdeuterated polystyrenes. We find that the gaussian conformation is retained parallel to the surfaces in all cases. Chain sizes equal the bulk value, within experimental uncertainty, although there is a systematic trend towards chain swelling in the thinnest films.

Computer simulations of polymer melts between impenetrable walls show that chain dimensions parallel to the surfaces are only slightly larger than in the bulk, and that the chain conformation in this direction remains gaussian[9–13]. In contrast to these ideas, recent self-diffusion measurements for confined polymeric systems are consistent with the notion that chain conformation is strongly modified[6,7]. Similarly, Frank *et al.*[8] have suggested that chain structure can be significantly affected in ultrathin films (that is, thickness $D \leqslant 100$ nm). Preliminary scattering studies by Russell[14] tentatively indicated that chain conformation is modified in the thin film geometry. Similarly, Reich and Cohen[15] found that polymers of high molecular mass exhibited long-range order (up to 10 μm) from the substrate. Based on these variable, often conflicting results, it is clear that even the most fundamental questions regarding the behaviour of polymer chains near surfaces is poorly understood.